Earth and Planetary Science Letters 602 (2023) 117968

Contents lists available at ScienceDirect

Earth and Planetary Science Letters

journal homepage: www.elsevier.com/locate/epsl

Shallow recycling of lower continental crust: The Mahoney Seamount at the Southwest Indian Ridge

Dominic Woelki [a,b,*], Vincent Salters [a], Christoph Beier [c], Henry Dick [e], Juergen Koepke [f], Rene Romer [d]

[a] National High Magnetic Field Laboratory, Department of Earth, Ocean and Atmospheric Science, Florida State University, Tallahassee, FL 32306, USA
[b] Westfälische Wilhelms Universität, Institut für Mineralogie, 48149 Münster, Germany
[c] Department of Geosciences and Geography, Research Programme of Geology and Geophysics (GeoHel), University of Helsinki, PO Box 64, 00014 Helsinki, Finland
[d] GeoZentrum Nordbayern, Friedrich-Alexander Universität (FAU) Erlangen-Nürnberg, Schlossgarten 5, D-91054 Erlangen, Germany
[e] Woods Hole Oceanographic Institution, Woods Hole, MA 02543, USA
[f] Institut für Mineralogie, Leibnitz Universität Hannover, Callinstrasse 3, 30167 Hannover, Germany

ARTICLE INFO

Article history:
Received 21 April 2022
Received in revised form 2 December 2022
Accepted 13 December 2022
Available online xxxx
Editor: R. Hickey-Vargas

Keywords:
Southwest Indian Ridge
off-axis
basalt
MORB
radiogenic isotopes
lower continental crust

ABSTRACT

The Mahoney Seamount is a recently discovered volcanic edifice located 4 km north of the ultra-slow spreading Southwest Indian Ridge (SWIR). The SWIR is one of the slowest spreading ridges worldwide with a full spreading rate of ~14 mm/year and low magmatic productivity. We report that highly vesicular basalts from the Mahoney Seamount have unradiogenic Nd-Hf together with radiogenic Sr isotopic compositions. Their distinct low $^{206}Pb/^{204}Pb$ isotope signature combined with high $^{207}Pb/^{204}Pb$ and $^{208}Pb/^{204}Pb$ is best explained by melting of a mantle that has been strongly influenced by stranded lower continental crust. The geographic distribution of the isotopic variability favors the idea of shallow recycling of lower continental crust isolated for a longer period contributing to melts forming Mahoney Seamount through off-axis fault systems. The isotopic composition of Mahoney Seamount lavas shares many characteristics with EM-1 sources and the DUPAL signature. Previous isotopic studies of the SWIR basalts proposed recycling of ancient subcontinental lithospheric mantle (SCLM) or pelagic sediments with oceanic crust to be responsible for this enriched isotopic signature. Lu/Hf and Sm/Nd ratios of pelagic sediments would result in decoupled $^{143}Nd/^{144}Nd$ and $^{176}Hf/^{177}Hf$ ratios. This decoupling is also observed in Ejeda-Bekily dikes from Madagascar, but those are believed to sample the SCLM dispersed in the Indian Ocean. However, Mahoney Seamount shows no decoupling in those isotopic systems and the restricted occurrence of the extreme lower continental crustal signature at Mahoney Seamount implies that the enriched isotopic signature has a different origin.

1. Introduction

The so-called DUPAL signature recognized in Indian Ocean ridge basalts (Dupré and Allègre, 1983; Hart, 1984) and EM-1 type mantle (Stracke et al., 2005) is characterized by low $^{206}Pb/^{204}Pb$, $^{143}Nd/^{144}Nd$, $^{176}Hf/^{177}Hf$ and high $^{207}Pb/^{204}Pb$, $^{208}Pb/^{204}Pb$ and $^{87}Sr/^{86}Sr$ ratios compared to ridge basalts from the Pacific and most of Atlantic mantle domains. This enriched isotopic composition is related to a time-integrated evolution of a component with high Th/U, Rb/Sr and low U/Pb, Sm/Nd and Lu/Hf dispersed in the Indian mantle domain (Hart, 1984). Basalts from the SWIR between 39° - 41°E with very low $^{206}Pb/^{204}Pb$ combined with low $^{143}Nd/^{144}Nd$, and $^{176}Hf/^{177}Hf$ have been interpreted to contain a component of either recycled lower continental crust, subcontinental lithospheric mantle (Escrig et al., 2004; Janney et al., 2005; Mahoney et al., 1992; Meyzen et al., 2005). Sediments recycled into the mantle billions of years ago can evolve to low $^{206}Pb/^{204}Pb$ combined with low $^{143}Nd/^{144}Nd$ (Stracke et al., 2003). Recycling of crustal material either occurs by subduction and deep recycling to the core-mantle boundary (e.g., ocean island basalts, OIBs), or by recycling into the shallow mantle during subduction erosion and/or crustal delamination (Clift et al., 2009; Willbold and Stracke, 2010) and later incorporation into upwelling flow of mantle.

Mahoney Seamount (named after geochemist Prof. J. J. Mahoney and discovered during cruise SO273 in 2020) is at 38.9°E north of SWIR. The SWIR is an ultra-slow spreading ridge (~14 mm/year, full spreading rate) extending from the Bouvet Fracture Zone for over 7000 km to the Rodriguez Triple junction (Patriat and

* Corresponding author.
E-mail address: dominicwoelki@tamu.edu (D. Woelki).

https://doi.org/10.1016/j.epsl.2022.117968
0012-821X/

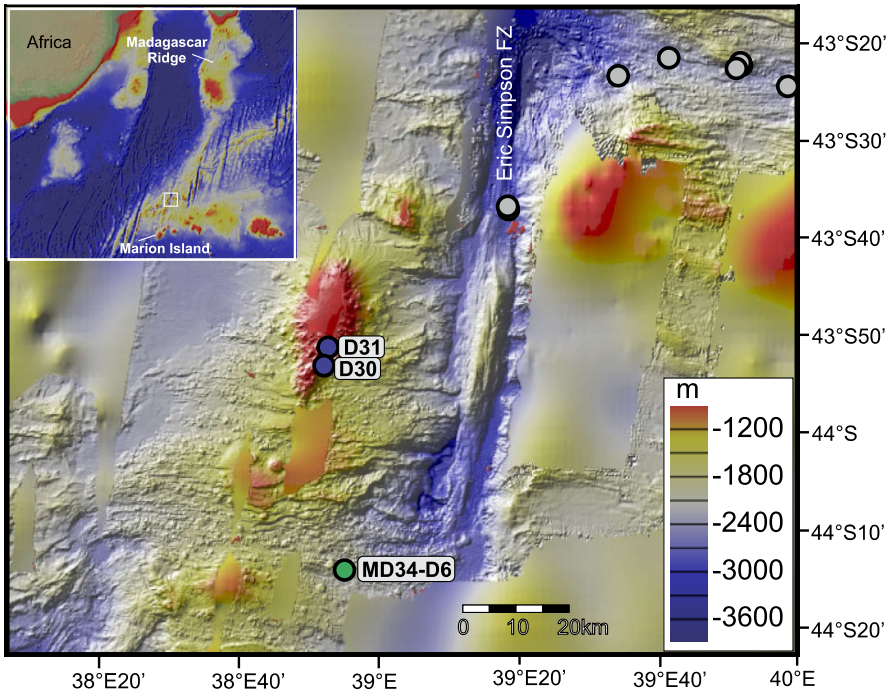

Fig. 1. Bathymetric map of Mahoney Seamount at the Southwest Indian Ridge west of Eric Simpson Fracture Zone. Blue circles D30 and D31 are dredge locations on Mahoney Seamount. Grey circles are dredge locations of 39-41°E basalts. Green circle is dredge location MD34-D6 of Marion influenced basalt (Janney et al., 2005; Mahoney et al., 1992; Meyzen et al., 2007, 2005). Panel A shows the location of the study area in the Indian Ocean, Madagascar Ridge, and Marion Island. Maps created with GeoMapApp together with high-resolution bathymetric data of expedition SO273 and MD121. (For interpretation of the colors in the figure(s), the reader is referred to the web version of this article.)

Segoufin, 1988). Mahoney Seamount is situated 40 km north of the ridge axis west of Eric Simpson Fracture Zone and protrudes 2 km above the seafloor with its top rising to 450 meters below sea level and its southern side covered by 500 to 800 m diameter parasitic cones. Mahoney Seamount has no corresponding edifice off-axis south of the SWIR (Fig. 1), is 33 km long by 18 km wide and is elongated in the spreading direction. R/V Sonne 273 in 2020 sampled Mahoney Seamount by two dredges which recovered 59 samples of highly vesicular basalts with abundant olivine and plagioclase phenocrysts. Twenty-five samples were selected for analysis based on their visible freshness and glass abundance.

2. Methods

Twenty-five lavas and glasses from Mahoney Seamount were analyzed geochemically for their major element, trace element, and isotopic composition. The complete data set is presented in supplementary Table S1. For whole rock analysis, samples were cut with a rock saw and alteration rims removed. The samples were washed thoroughly in deionized water to remove potential contamination by seawater, coarsely crushed, and reduced to powder with an agate mill. The powder was dried for 12 hours at 105 °C before being used for further major element and trace element analysis and preparation for Sr-Pb-Nd-Hf isotope determination.

2.1. Major elements

Major element analyses of the whole rock samples were carried out with a Spectro XEPOS He X-ray fluorescence spectrometer using fused glass beads after the method described by Woelki et al. (2018). Loss on ignition (LOI) was determined by weighing approximately 1 g of the sample before and after heating the samples for 12 hours at 1300 °C. The accuracy and precision of the major elements were determined by multiple measurements of the international rock standards BR and BE-N. The accuracy is generally better than 3.5% except for Na_2O and P_2O_5 where it is better than 6.4% and 9.4%, respectively. Precision is generally better than 1% except for Na_2O which is better than 3.3%.

Eleven lavas with fresh glass rinds were crushed and single 1-2 mm sized chips were hand-picked, cleaned in distilled water, embedded in epoxy resin, and polished for electron microprobe and laser ablation ICP-MS analyses. Fresh glasses were analyzed for major elements and trace elements. Analysis of the major elements (SiO_2, TiO_2, Al_2O_3, FeO_t, MnO, CaO, Na_2O, K_2O, P_2O_5 SO_3 and Cl) was carried out using a JEOL JXA-8200 Superprobe electron microprobe at the GeoZentrum Nordbayern (GZN), Friedrich-Alexander Universität Erlangen-Nürnberg, Germany. The microprobe was operated with an acceleration voltage of 15 kV, a beam current of 15 nA, and a defocused (10 µm) beam. Counting times were set to 20 s and 10 s for peaks and backgrounds for all elements, except for Cl where peak counting time was 40 s and background times were set to 20 s. Accuracy and precision were determined using international glass standards VG-2 and VG-A99 measured during each analytical session. For the VG-A99 standard, accuracy is better than 3.7% for all elements except MnO and P_2O_5, and precision is better than 3.3% except for MnO and P_2O_5 (Beier et al., 2018). The average values of 10 spot analyses on each sample and standard are presented in Table S1.

2.2. Trace elements

Trace element analyses of 16 selected whole rock samples were measured using a Thermo Fisher Scientific XSeries 2 Quadrupole Inductively Coupled Plasma Mass Spectrometer (ICP-MS) connected to an Aridus 2 membrane desolvating sample introduction system. Standard and sample powders were dissolved using nitric and hydrofluoric acid as reactants (Woelki et al., 2018). Repeated measurements of the international rock standard BHVO-2 yield an accuracy of better than 4% (2σ) for all analyzed elements.

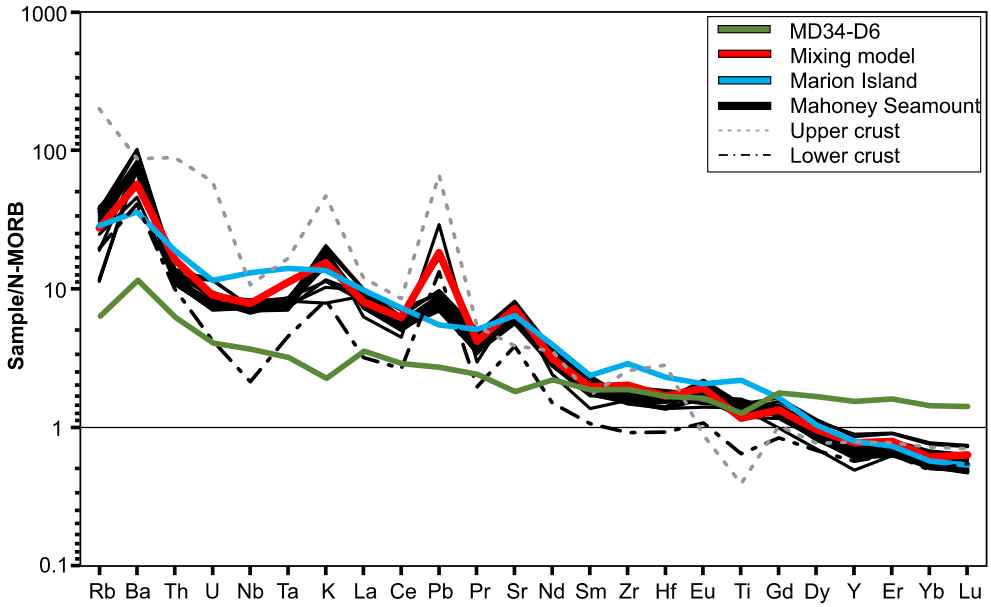

Fig. 2. Incompatible trace element patterns normalized to normal – mid-ocean ridge basalt (Sun and McDonough, 1989) of the MSL compared to REEBOX melting model of lower continental crust, depleted mantle and Marion Rise basalt (red line, details in discussion). Composition of average Marion Island basalts (Le Roex et al., 2012), MD34-D6 basalt (Janney et al., 2005) and lower and upper continental crust (Rudnick et al., 2003; Rudnick and Fountain, 1995) for comparison. Note the peaks at Ba, K, Pb, and Sr of the VOAB overlapping with continental crustal material.

Trace element contents of the glasses were analyzed by laser ablation inductively coupled plasma mass spectrometry (LA-ICPMS) using an Agilent 7900 s quadrupole system coupled to a Coherent GeoLas Pro MV 193 nm laser ablation system at the Department of Geosciences and Geography, Environmental and Mineralogical Laboratories (HelLabs) at the University of Helsinki in November 2020. Laser ablation spot sizes of 90 µm in diameter were used with a fluence of 10 J/cm2 at 10 Hz. The He carrier gas flow was set to 1050 ml/min. A set of 38 isotopes of 37 elements was measured (29Si, 39K, 43Ca, 44Ca, 45Sc, 47Ti, 51V, 52Cr, 60Ni, 63Cu, 66Zn, 71Ga, 85Rb, 88Sr, 89Y, 90Zr, 93Nb, 98Mo, 137Ba, 139La, 140Ce, 141Pr, 146Nd, 147Sm, 153Eu, 157Gd, 159Tb, 163Dy, 165Ho, 166Er, 169Tm, 172Yb, 175Lu, 178Hf, 181Ta, 208Pb, 232Th and 238U). The dwell time for Si, Ca, Ti, Rb, and Sr was set to 10 ms and 20 ms for all other elements, a 40-second washout prior and after each analytical period (50 seconds) was used to ensure sufficient background levels. Analyses of glasses and SRM NIST 612 as secondary reference materials measured as unknown were bracketed by measurements of the SRM NIST610 standard reference material every 15-20 analysis. The instrument was tuned to ThO/Th ratios of <0.3% and U/Th ratios of ~100%, doubly charged cations were tuned to <0.4% using SRM NIST610, and SRM NIST612 as unknown. Trace element concentrations were internally standardized using Si contents determined by EMP for the same grain domains. Repeated analysis of SRM NIST612 (n = 6) corrected using SRM NIST610 deviates less than 3% for most elements and 5% for K, Cr, Ba, Pr, Ho, Tm, and <8% for Cu and V, respectively relative to accepted values published in GEOREM for most elements. The long-term accuracy using SRM NIST612 (n = 426) deviates less than <3% from the published GEOREM values for all isotopes except for Mo, Ba, Pr, Ho, Tm which are <5%, respectively. SRM NIST 612 has a relative reproducibility standard deviation of less than 3% for all elements except for from the published GEOREM values.

2.3. Radiogenic isotopes

Seventeen basalts have been selected for Sr-Nd-Hf-Pb determination. Approximately 90 – 110 mg of sample powder were leached, dissolved, and processed through columns and measurement at the National High Magnetic Field Laboratory, Florida State University. The separates were leached in 5 ml 2.5N HCl and <30% H2O2 for 60 min at room temperature to remove any alteration products. The leached separates were rinsed several times with quartz sub-boiling distilled water. Subsequent dissolution and column chemistry was performed after procedures described by Stracke et al. (2003). Sr isotope compositions were measured by thermal ionization mass spectrometry (TIMS) using a Finnigan MAT 262 RPQ system. Measured value of the Eimer & Amend (E&A) SrCO3 standard is 87Sr/86Sr = 0.708000 ± 000007 (2σ, n = 6). The $^{87}Sr/^{86}Sr$ ratios are corrected for mass bias using $^{88}Sr/^{86}Sr = 0.1194$ and reported to the E&A SrCO3 standard of $^{87}Sr/^{86}Sr$ 0.708000. Blanks for Sr were <100 pg. Nd isotopes were measured using a Neptune multi-collector (MC-) ICP-MS system. The estimated uncertainties are based on repeated measurements of the standards. The measured value of the La Jolla standard is $^{143}Nd/^{144}Nd = 0.511799 \pm 0.000003$ (2σ, n = 19). The $^{143}Nd/^{144}Nd$ ratios are corrected for mass bias using a $^{146}Nd/^{144}Nd$ ratio of 0.7219 and are reported relative to La Jolla standard of 0.511850. Blanks for Nd were 10 pg.

For the digestions and Pb column chemistry only double distilled acids were used with dropper bottles to keep the blanks as low as possible. For the separation of Pb, the dissolved samples were loaded on 100 µl Sr-Spec resin columns and washed with 1M HCl. The Pb was collected using 6M HCl. Lead isotope measurements were carried out on a Thermo-Fisher Neptune MC-ICP-MS using a $^{207}Pb/^{204}Pb$ double spike to correct for instrumental mass fractionation. The double spike, with a $^{207}Pb/^{204}Pb$ ratio of 0.8135, was calibrated against a solution of the NBS982 equal atom Pb standard. Samples were diluted with 2% HNO3 to a concentration of ~20 ppb, and an aliquot of this solution spiked to obtain a $^{208}Pb/^{204}Pb$ ratio of about 1. Spiked and unspiked sample solutions were introduced into the plasma via a Cetac Aridus desolvating nebulizer and measured in static mode. Interference of ^{204}Hg on mass 204 was corrected by monitoring ^{202}Hg. An exponential mass fractionation correction was applied offline using the iterative method of Compston and Oversby (1969), the correction was typically 4.5 permil per amu. Twenty measurements of the NBS981 Pb isotope standard (measured as an unknown) through-

out this study gave $^{206}Pb/^{204}Pb$, $^{207}Pb/^{204}Pb$, $^{208}Pb/^{204}Pb$ ratios of 16.9459, 15.5019, and 36.7301, respectively. The Pb blanks are generally below 30 pg. The results for all samples can be found in Supplementary Table 1.

3. Results

R/V Sonne SO273 *Marion Rise* in 2020 recovered Mahoney Seamount lavas (MSL) by two dredges (D30, D31; Fig. 1). They recovered highly vesicular basalts with abundant olivine and plagioclase phenocrysts. We have analyzed the major and trace element abundances and Sr-Nd-Hf-Pb isotopic ratios (Figs. 2-3; see appendix for data) of fresh basalts (LOI <1.4 wt.%, except for one sample) and glasses. The glasses have low Cl/K_2O ratios of <0.02 overlapping with mantle values (~0.09) even at high Ba/Th, showing their composition was not influenced by seawater contamination (Michael and Schilling, 1989). Whole-rock analyses overlap with glass analysis, indicating that their compositions have not been changed by seawater contamination. The recovered MSL range in composition from basalt to basaltic andesite with MgO contents of 7.6 – 5.1 wt.%, K_2O of 0.57 – 1.49 wt.% and TiO_2 of 1.5 – 2.0 wt.%. Lavas from nearby Marion Island (Le Roex et al., 2012) overlap in MgO and K_2O, but tend to lower TiO_2. N-MORB normalized (Sun and McDonough, 1989) incompatible trace-element patterns show an enrichment of highly incompatible elements and depletion of Heavy Rare Earth Elements (HREE), with elevated concentrations of Ba, K, Sr, and Pb similar to global OIB and Marion Island (Fig. 2). The MSL however display lower Nb, Ta, Th, Zr and Ti contents compared to Marion Island basalts and have higher Ba/Nb (18.6 – 33.5) and Ba/Th (213 – 385) ratios, respectively (Fig. 2 & 5). The Ba/Th ratios are approximately three times higher than most OIB (~87) (Stracke et al., 2003; Sun and McDonough, 1989) including EM-1 type OIBs like Pitcairn Seamounts (50 - 100; Stracke et al., 2003) (Fig. 5) but are comparable to the Afanasy-Nikitin Rise (253 – 264) (Borisova et al., 1996; Homrighausen et al., 2021; Mahoney et al., 1996). The Afanasy-Nikitin Rise is the southern terminus of the aseismic 85°E Ridge in the northern Indian Ocean, south of India (Homrighausen et al., 2021; Mahoney et al., 1996).

In radiogenic isotope space, the MSL have distinct low $^{143}Nd/^{144}Nd$, $^{176}Hf/^{177}Hf$ and high $^{87}Sr/^{86}Sr$ (Fig. 3). They have extreme Pb-isotopic composition with low $^{206}Pb/^{204}Pb$, falling well left of the geochron with high $^{207}Pb/^{204}Pb$ (Fig. 3), and intermediate $^{208}Pb/^{204}Pb$ for their $^{206}Pb/^{204}Pb$. These geochemical characteristics overlap with EM-1 type OIB, and their closest analogues in Nd-Sr-Pb isotopic composition are the Afanasy-Nikitin Rise basalts (Homrighausen et al., 2021; Mahoney et al., 1996). SWIR basalts (MORB) at 39° – 41°E, the ridge nearest to Mahoney Seamount, fall above the $^{143}Nd/^{144}Nd$ - $^{176}Hf/^{177}Hf$ mantle array tending towards higher $^{176}Hf/^{177}Hf$ isotopic ratios (Fig. 4; Janney et al., 2005; Mahoney et al., 1992, 1996; Meyzen et al., 2007, 2005). Lavas from the Afanasy-Nikitin Rise and the 39° – 41°E SWIR both show unradiogenic Pb-isotope compositions.

4. Discussion

4.1. Origin of the distinct composition of Mahoney Seamount

The origin of the enriched component in Indian MORB has been discussed extensively over the last decades, e.g., delaminated subcontinental lithospheric mantle (SCLM) (Tatsumi, 2000), recycled oceanic crust with sediments (Hofmann and White, 1982), pelagic sediments and continental lower and upper crustal material (Janney et al., 2005; Meyzen et al., 2005; Willbold and Stracke, 2010). The MSL shows some of the most pronounced characteristics of the Indian Ocean component and thus allow us to define the origin of this component in this area.

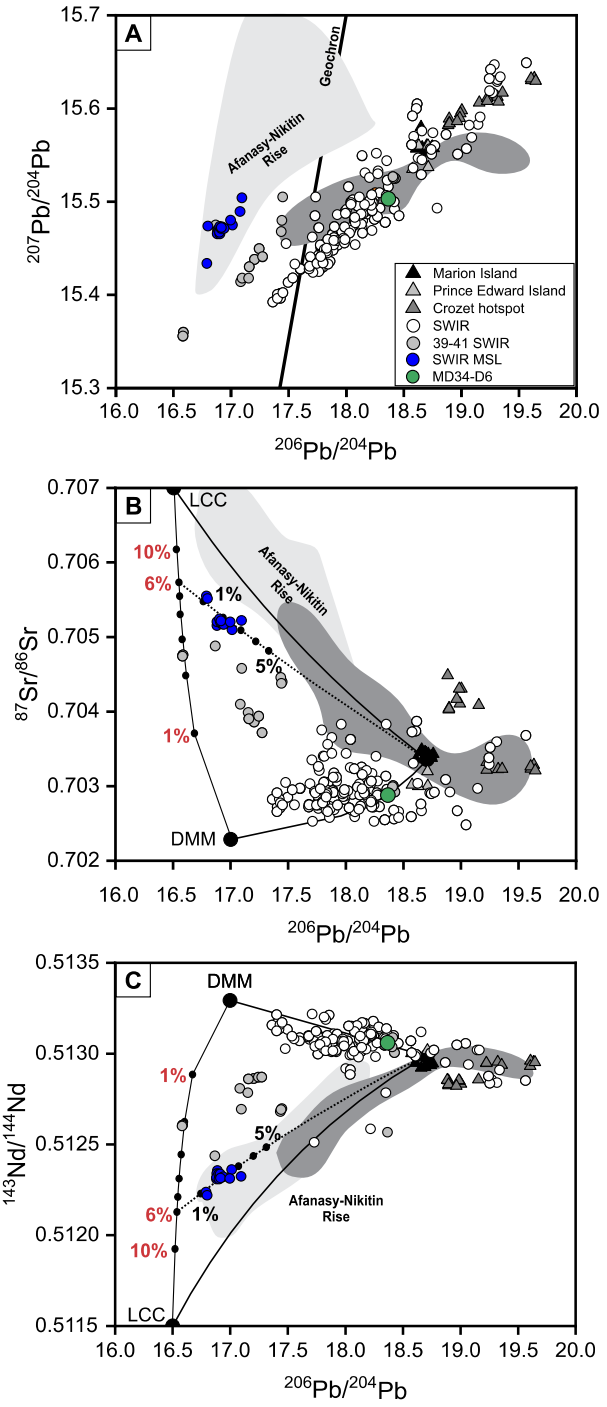

Fig. 3. Isotopic variation of MSL compared to Indian MORB, 39-41°E basalts (gray circle), MD34-D6 basalt (green circle) and Marion, Prince Edward, and Crozet plume lavas. (A) $^{207}Pb/^{204}Pb$, (B) $^{87}Sr/^{86}Sr$, (C) $^{143}Nd/^{144}Nd$ vs. $^{206}Pb/^{204}Pb$. Compositions of the three endmembers are lower continental crust (LCC), depleted MORB mantle (DMM), and Marion plume together with bulk mixing lines. Endmember compositions are reported in the supplemental material. Red numbers indicate percentage of LCC mixed with DMM and black numbers indicate percentage of mixed LCC-DMM with Marion plume. Afanasy-Nikitin Rise (light gray field) (Homrighausen et al., 2021; Mahoney et al., 1996) and Pitcairn EM-1 lavas (dark gray field) (Stracke et al., 2003) for comparison. Data of Indian MORB along the SWIR are from the PetDB database (https://search.earthchem.org/, Accessed September 2021).

Subducted pelagic sediments would evolve to highly radiogenic $^{87}Sr/^{86}Sr$, and unradiogenic $^{206}Pb/^{204}Pb$, and $^{143}Nd/^{144}Nd$. Pelagic sediments also have deficiencies in Zr and Hf, and thus tend to have high Lu/Hf and low Sm/Nd (Vervoort et al., 2011), which will

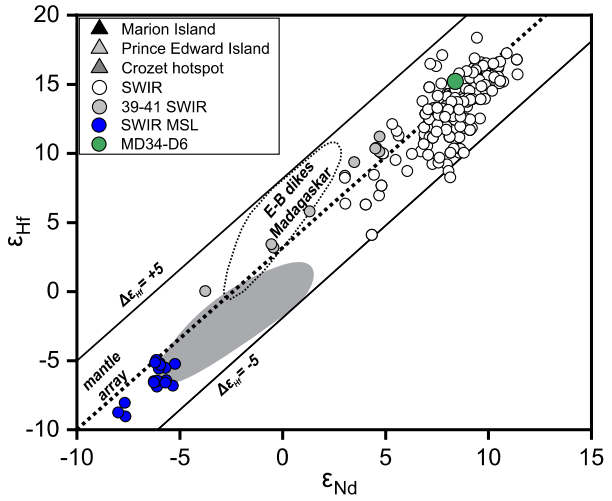

Fig. 4. Plot of ε_{Hf} vs ε_{Nd} of the MSL compared to MORB along the SWIR, 39 – 41°E basalts and Ejeda-Bekily dikes from Madagascar (Mahoney et al., 1991; Storey et al., 1997). The mantle array (dashed line) represents the regression line of Vervoort et al. (2000) of oceanic basalts. Lines labeled $\Delta\varepsilon_{Hf}$ is the offset 5 ε_{Hf} units below and above the mantle array. Pitcairn EM-1 lavas (dark gray field) (Stracke et al., 2003). Data sources as in Fig. 3.

result in decoupling of $^{143}Nd/^{144}Nd$ and $^{176}Hf/^{177}Hf$ ratios, and rules them out as a possible source in the MSL as the Hf and Nd isotopes at Mahoney Seamount are correlated and fall below the mantle array (Fig. 4; Rehka and Hofmann, 1997).

Peridotite xenoliths from southern Africa have shown that subcontinental lithospheric mantle (SCLM) has radiogenic $^{87}Sr/^{86}Sr$, unradiogenic $^{206}Pb/^{204}Pb$, and decoupled Hf-Nd isotope systematics with radiogenic Hf (Simon et al., 2007). However, none of the Southern African peridotite xenoliths have $^{206}Pb/^{204}Pb$ low enough to explain either the 39° – 41°E basalts or the MSL (Hawkesworth et al., 1990; Kramers, 1977; Kramers et al., 1983). The Ejeda-Bekily dikes in Madagascar have been interpreted to be SCLM melts because of their high $^{176}Hf/^{177}Hf$ and due to their similarity in Sr-Nd isotopes. It has been argued that SCLM is the origin of the enriched isotopic composition at the 39° – 41°E ridge segment (Janney et al., 2005; Mahoney et al., 1992, 1991; Storey et al., 1997). However, opposite to the 39 – 41°E basalts the MSL lie below the Hf-Nd mantle array and thus require a different source contribution (Fig. 4). We conclude that SCLM and subducted pelagic sediments can both be ruled out for the origin of the MSL.

Involvement of recycled oceanic crust in combination with sediments and recycled crustal material could potentially explain the MSL. While subduction of pure oceanic crust will result in a HIMU-type component with high $^{206}Pb/^{204}Pb$ ratios (Zindler and Hart, 1986), oceanic crust with variable amounts of global subducting sediment (GLOSS) can evolve to unradiogenic $^{206}Pb/^{204}Pb$, $^{143}Nd/^{144}Nd$, and $^{176}Hf/^{177}Hf$ and radiogenic $^{87}Sr/^{86}Sr$ (Janney et al., 2005; Willbold and Stracke, 2010). GLOSS is mainly dominated by terrigenous material and thus its composition is biased towards the upper continental crust (Plank and Langmuir, 1998). Incompatible trace elements are very variable in the continental crust, but upper crust generally has high Rb/Sr and thus evolves to high $^{87}Sr/^{86}Sr$ ratios (Rudnick et al., 2003; Stracke et al., 2003; Willbold and Stracke, 2010). The MSL have high $^{87}Sr/^{86}Sr$ ratios greater than 0.705 (Fig. 5), and are higher than those from the Marion hotspot, but lower than many OIBs associated with "EM-type" mantle components worldwide (Stracke et al., 2003; Willbold and Stracke, 2010). Willbold and Stracke (2010) showed that most OIBs with $^{87}Sr/^{86}Sr$ ratios greater than 0.706 also have Eu/Eu* < 1 ($Eu^* = (Sm_N \times Gd_N)^{1/2}$), whereas OIBs with $^{87}Sr/^{86}Sr$ ratios lower than 0.706 have Eu/Eu* ≥ 1. The Eu/Eu* in the MSL (1.04 – 1.2)

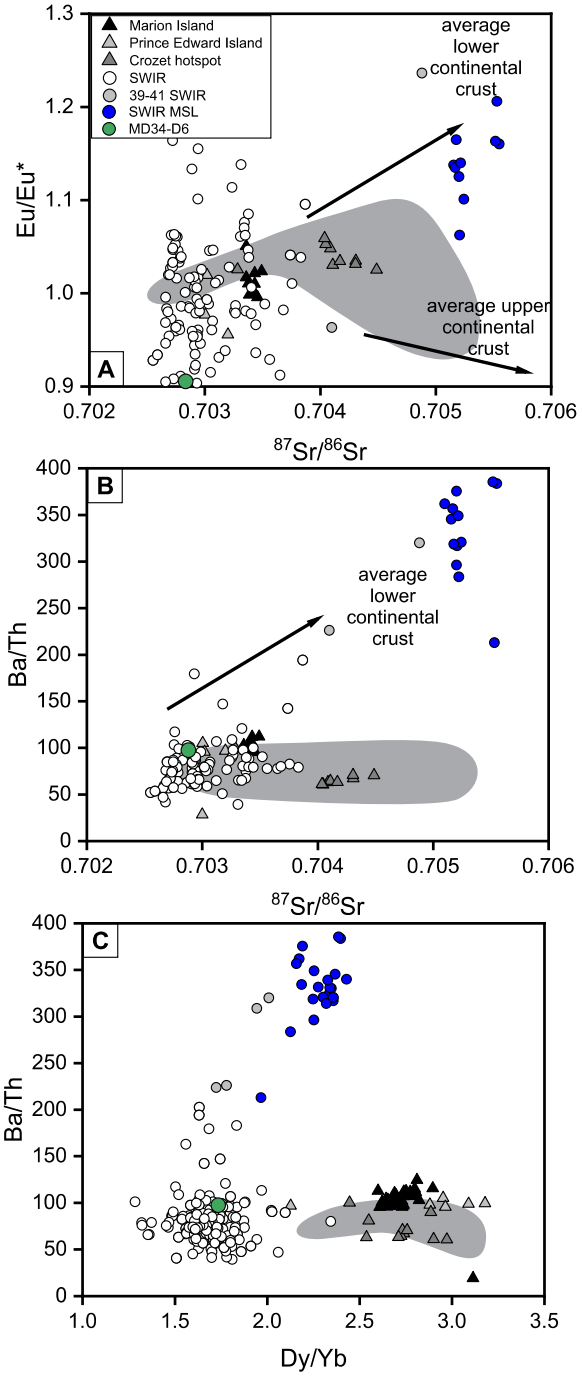

Fig. 5. Variations of (A) $^{87}Sr/^{86}Sr$ with Eu/Eu* (Eu* is the chondrite-normalized Eu concentration derived by interpolation between the chondrite-normalized Sm_N and Gd_N concentrations ($Eu^* = (Sm_N \times Gd_N)^{1/2}$)) and (B) Ba/Th with $^{87}Sr/^{86}Sr$ of the MSL. Most MSL have Eu/Eu* ratios >1 and high $^{87}Sr/^{86}Sr$, indicating lower continental crust contribution. (C) The Mahoney lavas have intermediate Dy/Yb between most Indian MORB and plume related lavas (Marion Island, Prince Edward Island, Crozet) at high Ba/Th ratios, implying a different origin of the high Dy/Yb in the MSL Pitcairn EM-1 lavas (dark gray field) (Stracke et al., 2003). Data sources as in Fig. 3.

is not correlated with Mg# and likely source related. Several studies found that lower continental crust typically has Eu/Eu* > 1, whereas upper continental crust has Eu/Eu* < 1, related to either depletion or excess of plagioclase in the enriched source component (Rudnick et al., 2003). Eu/Eu* ≥ 1 and high Ba/Th could also be explained by the interaction of melts with plagioclase-rich lower oceanic crustal cumulates, however low Cl/K_2O and differ-

ences in $^{206}Pb/^{204}Pb$ - $^{207}Pb/^{204}Pb$, and $^{87}Sr/^{86}Sr$ isotopic compositions (Holm, 2002) cannot be explained this way. The MSL all show Eu/Eu* > 1 at higher $^{207}Pb/^{204}Pb$ and low $^{206}Pb/^{204}Pb$ at high Ba/Th. This is consistent with a lower continental crust (Ba/Th > 250) compared to a upper continental crust (Ba/Th ~50) component (Fig. 5; Rudnick et al., 2003) and confirms previous studies that argued for the absence of a subducted sediment component in the 39 – 41°E basalts based on the U-Th-Pb systematics (Meyzen et al., 2005). We conclude that lower crustal material is most likely responsible for the unradiogenic $^{206}Pb/^{204}Pb$, $^{143}Nd/^{144}Nd$, and $^{176}Hf/^{177}Hf$ and radiogenic $^{87}Sr/^{86}Sr$ signature at Mahoney Seamount.

The MSL and adjacent SWIR basalts range to higher $^{206}Pb/^{204}Pb$ than depleted MORB mantle (DMM) and lower continental crust, indicating a third component must contribute (Fig. 3). Indian MORB are thought to contain a component with moderate $^{206}Pb/^{204}Pb$, high $^{207}Pb/^{204}Pb$, $^{208}Pb/^{204}Pb$, and $^{87}Sr/^{86}Sr$ at low $^{143}Nd/^{144}Nd$ and $^{176}Hf/^{177}Hf$ related to plume material in the Indian Ocean (Janney et al., 2005; Meyzen et al., 2005; Stracke et al., 2005). The composition of the nearby Marion hotspot as a third component can explain the MSL compositions and has been argued to influence the SWIR in this area (Le Roex et al., 2012; Mahoney et al., 1992; Meyzen et al., 2005).

The basalt compositions were modeled with the REEBOX PRO (Brown and Lesher, 2016) adiabatic decompression melting model with passive upwelling. Inputs for initial lithologic abundances for anhydrous peridotite, silica-saturated pyroxenite and silica-undersaturated pyroxenite are DMM, lower continental crust (Meyzen et al., 2005; Rudnick et al., 2003) and Marion island basalt (Le Roex et al., 2012), respectively. We assumed mantle potential temperature of 1330 °C and a lithospheric thickness of ~5 km consistent with 7.5 mm half-spreading rate. In bulk isotopic mixing calculations (Fig. 2), most of the SWIR MORB can be explained by a mixture of a depleted mantle, plume influenced material (e.g., Marion plume) and contributions of lower continental crustal material. The MSL lava trace element compositions can be explained by mixing DMM with a Marion plume component (6%) and a larger amount of lower continental crustal material (10%) (Fig. 2), whereas the isotopic compositions constrain the Marion plume and lower continental crust contribution to 2 – 3% and 6%, respectively (Fig. 3) and is in good agreement taking the potential variability of source components into account. MSL and nearby Indian MORB differ by the contribution of lower continental crust needed to explain the extreme isotopic composition. Modeling endmember compositions are detailed in the supplemental material, further details on the modeling can be found in Brown and Lesher (2016).

4.2. Deep versus shallow recycling of lower continental crust

An important question is whether the crustal component present in MSL was incorporated through upwelling of deep plume material from the nearby Marion plume or is entrained into the mantle through shallow recycling of lower continental crust during the breakup of Gondwana (Escrig et al., 2004; Janney et al., 2005; Mahoney et al., 1992; Meyzen et al., 2005; Zhou and Dick, 2013). Previous studies (Mahoney et al., 1992; Meyzen et al., 2005) showed that the influence of the Marion plume at the ridge is strongest in the region between 36 - 39°E (Fig. 1, 3). On-ridge basalt MD34-D6 only 40 km south of the MSL is strongly influenced by the Marion plume and shows no evidence of lower crust involvement (Fig. 2; Mahoney et al., 1992; Meyzen et al., 2005). At 39° - 41°E, between the Eric Simpson and Discovery II fracture zone, a lower continental crust component (i.e., unradiogenic $^{206}Pb/^{204}Pb$, $^{143}Nd/^{144}Nd$, and $^{176}Hf/^{177}Hf$ and radiogenic $^{87}Sr/^{86}Sr$) appears (Janney et al., 2005; Mahoney et al., 1992; Meyzen et al., 2005). The variation in source components in this area could be explained if the components are unevenly distributed in the Marion plume and the lower continental crustal component occurs only to the east of the Eric Simpson fracture zone. The maximum amount of a lower continental crustal component at Mahoney Seamount on the opposite of the spreading axis as Marion Island makes this unlikely. The origin of the lower crust component north of the ridge is further indicated by the spreading axis at ~38.8°E, directly between Mahoney Seamount and Marion Island which shows larger contributions of the Marion plume component compared to the MSL (Fig. 2; Mahoney et al., 1992; Meyzen et al., 2005). The lower continental crust component is most prevalent in the MSL, north of the ridge axis, and absent at the on-axis basalts MD34-D6. Thus, we suggest that the lower continental crustal material originates from a shallow recycling into the upper asthenosphere as opposed to a deep contribution from the Marion mantle plume.

The lower continental crustal component (i.e., unradiogenic $^{206}Pb/^{204}Pb$, $^{143}Nd/^{144}Nd$, and $^{176}Hf/^{177}Hf$ and radiogenic $^{87}Sr/^{86}Sr$) occurs at the intersection of the SWIR and the extension of the Madagascar Ridge, which is thought to be the late Cretaceous-Tertiary expression of the Marion plume (Fig. 1; Duncan et al., 1990). The Ejeda-Bekily dikes are evidence of this plume activity beneath Indo-Madagascar between 130 and 85 Ma ago, when the plume was interacting with the SCLM and forming melts similar to the 39 – 41°E basalts at the SWIR (Duncan et al., 1990; Mahoney et al., 1992, 1991). Likely the SCLM together with lower continental crustal material eroded due to the Marion plume activity. The higher density of lower crust compared to the underlying asthenosphere caused delamination and sinking into the mantle (Jull and Kelemen, 2001). This process is proposed to occur in arcs, rifted margins and continental masses with high rates of extension (Clift and Vannucchi, 2004; Jull and Kelemen, 2001; Rudnick et al., 2003). These type of conditions were probably met during the breakup of Gondwana (Mahoney et al., 1992). If lower crust sank into the shallow mantle during continental breakup and Marion plume activity was directly involved, this material would be transported with the mantle flow either away or towards the developing spreading axis. No exact information of the location of the Marion Plume relative to the spreading axis is available, however the limited occurrence of the lower continental crust on only one side of the spreading axis favors the plume position away from the spreading axis. Thus, we speculate that lower continental crustal material observed in the MSL was delaminated and sank to a depth as blocks relatively isolated for a longer period of time and subsequently incorporated in upward flow due to rifting and spreading (Fig. 6).

4.3. Eruption mechanism

The occurrence of more exotic compositions such as the MSL is likely representing sampling a smaller mantle domain related to the ultra-slow spreading rate and the extensive segmentation of the ridge. Both, segmentation, and slow spreading result in thicker lithosphere and decreased melting and increased average depth of melting (Dick et al., 2003; Fox and Gallo, 1984; Reid and Jackson, 1981). At ridge-transform intersections, the ridge is cooled by old and thick lithosphere across the transform fault: the “transform cold-edge effect” (Fox and Gallo, 1984). This effect is strongest at large transform offsets at ultraslow spreading rates like at Eric Simpson fracture zone next to Mahoney Seamount (Fig. 1; Fox and Gallo, 1984). Models have shown that crustal production decrease towards transforms (Bonatti et al., 2001), which is evidenced by the widespread occurrence of exposed peridotite at the Marion Rise. The high vesicularity of the MSL indicate the presence of volatiles in the source as well as decreased degree of melting. Melting in the presence of residual garnet is indicated by higher

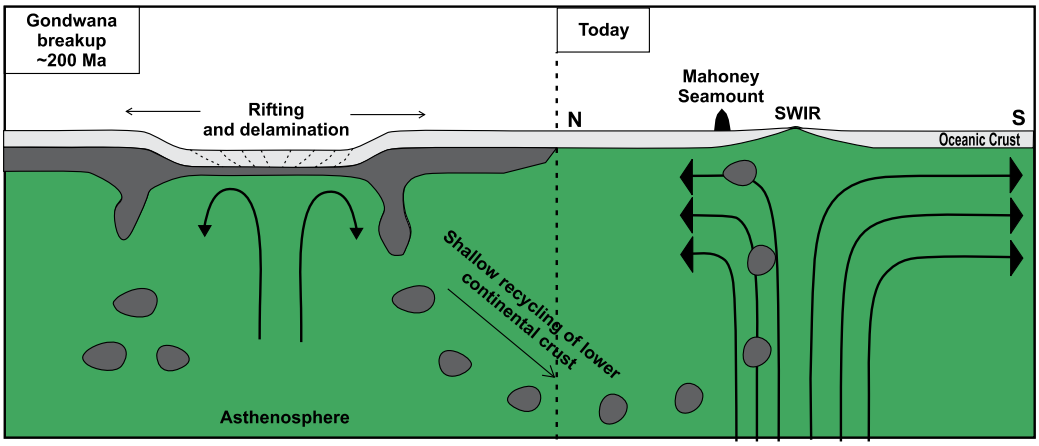

Fig. 6. Schematic model of the process of sinking of lower continental crustal (LCC) material during rifting and Gondwana breakup ~200 Ma (Mahoney et al., 1992) and recycling at the SWIR today. During rifting, LCC material was eroded and sank to depths where the crustal material could stay isolated for longer periods of time. LCC material has been transported to the now established spreading center by upwelling, contributing to Mahoney Seamount lavas at the northern side of the ridge.

Dy/Yb ratios of the Mahoney lavas (2.3 – 2.8) compared to Indian MORB (<2.0) (Janney et al., 2005; Ligi et al., 2005; Meyzen et al., 2005). These melts are less efficiently extracted on-axis as at a slightly cooler and thicker lithosphere (Standish and Sims, 2010). Furthermore, seismic imaging shows that long-lived rift bounding faults at the Mid-Atlantic ridge penetrating the melt injection zone at the brittle-ductile transition zone (Demartin et al., 2007) and thicker lithosphere would deepen the brittle-ductile transition zone, fault penetration depth and generating melt permeable pathways through the crust (Standish and Sims, 2010), allowing melts to be extracted off-axis.

5. Conclusions

The material recycled at the Mahoney Seamount shares many characteristics with the EM-1 enriched mantle component and the so-called DUPAL signature found in various spreading centers and ocean islands worldwide. The obvious occurrence of this lower continental crustal component can be related to the unique location of the Mahoney Seamount on the extension of the Madagascar Ridge. However, the shallow recycling of lower continental crustal material is not unique to this location and is a more common process often associated with continental break-up. This has been argued to be responsible for the formation of the Afanasy-Nikitin Rise in the Eastern Indian Ocean (Mahoney et al., 1996) and the Christmas Island Seamount Province which probably formed during the breakup of West Burma from Australia and India (Hoernle et al., 2011). These observations imply that continental break-up could play an important role in delamination and foundering of lower continental crust into the shallow asthenosphere and recycling during upwelling. Whether delaminated and widely dispersed lower continental crust is responsible for enriched signatures like DUPAL needs more detailed knowledge of the composition of the lower continental crust together with information about the recycling and dispersion in the mantle.

CRediT authorship contribution statement

Dominic Woelki: Conceptualization, Methodology, Investigation, Writing – Original Draft, Visualization, Supervision.

Vincent Salters: Conceptualization, Writing – Review & Editing, Funding acquisition.

Christoph Beier: Investigation, Writing – Review & Editing, Funding acquisition.

Henry Dick: Funding acquisition, Writing – Review & Editing.

Juergen Koepke: Writing – Funding acquisition, Writing – Review & Editing.

Rene Romer: Investigation.

Declaration of competing interest

The authors declare that they have no known competing financial interests or personal relationships that could have appeared to influence the work reported in this paper.

Data availability

Data will be made available on request.

Acknowledgements

We thank Afi Sachi Kocher, Alexandra Zeh, and Julia Wenske for help during sample preparation and measurement. We thank Andreas Stracke and Felix Genske for useful discussions. We would also thank captain Lutz Mallon, the crew and scientists of RV Sonne for their help and support during SO273 cruise *Marion Rise* and the ordeal of a COVID-related return back to Germany. The cruise was financed by Bundesministerium für Bildung und Forschung (03G0273E, 03G0273D). We acknowledge funding from NSF grant OCE-1657826 (to V.J.M.S.). Part of this work was performed at the National High Magnetic Field Laboratory, which is supported by NSF Cooperative Agreement no. DMR-1157490 and DMR-1644779 and the state of Florida.

Appendix A. Supplementary material

Supplementary material related to this article can be found online at https://doi.org/10.1016/j.epsl.2022.117968.

References

Beier, C., Brandl, P.A., Lima, S.M., Haase, K.M., 2018. Tectonic control on the genesis of magmas in the New Hebrides arc (Vanuatu). Lithos 312, 290–307. https://doi.org/10.1016/j.lithos.2018.05.011.

Bonatti, E., Brunelli, D., Fabretti, P., Ligi, M., Portaro, R.A., Seyler, M., 2001. Steady-state creation of crust-free lithosphere at cold spots in mid-ocean ridges. Geology 29 (11), 979–982. https://doi.org/10.1130/0091-7613(2001)029<0979:SSCOCF>2.0.CO;2.

Borisova, A.Y., Sushchevskaya, N., Nikulin, V., Belyatskii, B., Ovchinnikova, G., Levskii, L., 1996. Late alkaline lavas of the Ob and Lena Seamounts (Conrad Rise, Indian Ocean): geochemistry and characteristics of mantle sources. Geochem. Int. 34 (6), 503–517.

Brown, E.L., Lesher, C.E., 2016. REEBOX PRO: a forward model simulating melting of thermally and lithologically variable upwelling mantle. Geochem. Geophys. Geosyst. 17 (10), 3929–3968. https://doi.org/10.1002/2016GC006579.
Clift, P., Vannucchi, P., 2004. Controls on tectonic accretion versus erosion in subduction zones: implications for the origin and recycling of the continental crust. Rev. Geophys. 42 (2). https://doi.org/10.1029/2003RG000127.
Clift, P.D., Vannucchi, P., Morgan, J.P., 2009. Crustal redistribution, crust–mantle recycling and Phanerozoic evolution of the continental crust. Earth-Sci. Rev. 97 (1–4), 80–104. https://doi.org/10.1016/j.earscirev.2009.10.003.
Compston, W., Oversby, V., 1969. Lead isotopic analysis using a double spike. J. Geophys. Res. 74 (17), 4338–4348. https://doi.org/10.1029/JB074i017p04338.
Demartin, B.J., Sohn, R.A., Pablo Canales, J., Humphris, S.E., 2007. Kinematics and geometry of active detachment faulting beneath the Trans-Atlantic Geotraverse (TAG) hydrothermal field on the Mid-Atlantic Ridge. Geology 35 (8), 711–714. https://doi.org/10.1130/G23718A.1.
Dick, H.J., Lin, J., Schouten, H., 2003. An ultraslow-spreading class of ocean ridge. Nature 426 (6965), 405–412. https://doi.org/10.1038/nature02128.
Duncan, R., Backman, J., Peterson, L., 1990. The volcanic record of the Reunion hotspot. In: Proceedings of the Ocean Drilling Program, Scientific Results, vol. 115. Ocean Drilling Program, Texas A&M University, College Station, TX, pp. 3–10.
Dupré, B., Allègre, C.J., 1983. Pb–Sr isotope variation in Indian Ocean basalts and mixing phenomena. Nature 303 (5913), 142–146. https://doi.org/10.1038/303142a0.
Escrig, S., Capmas, F., Dupré, B., Allègre, C., 2004. Osmium isotopic constraints on the nature of the DUPAL anomaly from Indian mid-ocean-ridge basalts. Nature 431 (7004), 59–63. https://doi.org/10.1038/nature02904.
Fox, P.J., Gallo, D.G., 1984. A tectonic model for ridge-transform-ridge plate boundaries: implications for the structure of oceanic lithosphere. Tectonophysics 104 (3–4), 205–242. https://doi.org/10.1016/0040-1951(84)90124-0.
Hart, S.R., 1984. A large-scale isotope anomaly in the Southern Hemisphere mantle. Nature 309 (5971), 753–757. https://doi.org/10.1038/309753a0.
Hawkesworth, C., Erlank, A., Kempton, P., Waters, F., 1990. Mantle metasomatism: isotope and trace-element trends in xenoliths from Kimberley, South Africa. Chem. Geol. 85 (1–2), 19–34. https://doi.org/10.1016/0009-2541(90)90121-M.
Hoernle, K., Hauff, F., Werner, R., van den Bogaard, P., Gibbons, A., Conrad, S., Müller, R., 2011. Origin of Indian Ocean Seamount Province by shallow recycling of continental lithosphere. Nat. Geosci. 4 (12), 883–887. https://doi.org/10.1038/ngeo1331.
Hofmann, A.W., White, W.M., 1982. Mantle plumes from ancient oceanic crust. Earth Planet. Sci. Lett. 57 (2), 421–436. https://doi.org/10.1016/0012-821X(82)90161-3.
Holm, P.M., 2002. Sr, Nd and Pb isotopic composition of in situ lower crust at the Southwest Indian Ridge: results from ODP Leg 176. Chem. Geol. 184 (3–4), 195–216. https://doi.org/10.1016/S0009-2541(01)00364-3.
Homrighausen, S., Hoernle, K., Wartho, J.-A., Hauff, F., Werner, R., 2021. Do the 85°E Ridge and Conrad Rise form a hotspot track crossing the Indian Ocean?. Lithos 398, 106234. https://doi.org/10.1016/j.lithos.2021.106234.
Janney, P., Le Roex, A., Carlson, R., 2005. Hafnium isotope and trace element constraints on the nature of mantle heterogeneity beneath the central Southwest Indian Ridge (13 E to 47 E). J. Petrol. 46 (12), 2427–2464. https://doi.org/10.1093/petrology/egi060.
Jull, M., Kelemen, P.B., 2001. On the conditions for lower crustal convective instability. J. Geophys. Res., Solid Earth 106 (B4), 6423–6446. https://doi.org/10.1029/2000JB900357.
Kramers, J., 1977. Lead and strontium isotopes in Cretaceous kimberlites and mantle-derived xenoliths from Southern Africa. Earth Planet. Sci. Lett. 34 (3), 419–431. https://doi.org/10.1016/0012-821X(77)90053-X.
Kramers, J., Roddick, J., Dawson, J., 1983. Trace element and isotope studies on veined, metasomatic and "MARID" xenoliths from Bultfontein, South Africa. Earth Planet. Sci. Lett. 65 (1), 90–106. https://doi.org/10.1016/0012-821X(83)90192-9.
Le Roex, A., Chevallier, L., Verwoerd, W., Barends, R., 2012. Petrology and geochemistry of Marion and Prince Edward Islands, Southern Ocean: magma chamber processes and source region characteristics. J. Volcanol. Geotherm. Res. 223, 11–28. https://doi.org/10.1016/j.jvolgeores.2012.01.009.
Ligi, M., Bonatti, E., Cipriani, A., Ottolini, L., 2005. Water-rich basalts at mid-ocean-ridge cold spots. Nature 434 (7029), 66–69. https://doi.org/10.1038/nature03264.
Mahoney, J., Le Roex, A., Peng, Z., Fisher, R., Natland, J., 1992. Southwestern limits of Indian Ocean Ridge Mantle and the origin of low 206Pb/204Pb mid-ocean ridge basalt: Isotope systematics of the central Southwest Indian Ridge (17°–50°E). J. Geophys. Res., Solid Earth 97 (B13), 19771–19790. https://doi.org/10.1029/92JB01424.
Mahoney, J., Nicollet, C., Dupuy, C., 1991. Madagascar basalts: tracking oceanic and continental sources. Earth Planet. Sci. Lett. 104 (2–4), 350–363. https://doi.org/10.1016/0012-821X(91)90215-4.
Mahoney, J., White, W., Upton, B., Neal, C., Scrutton, R., 1996. Beyond EM-1: lavas from Afanasy-Nikitin rise and the Crozet archipelago, Indian Ocean. Geology 24 (7), 615–618. https://doi.org/10.1130/0091-7613(1996)024<0615:BELFAN>2.3.CO;2.
Meyzen, C.M., Blichert-Toft, J., Ludden, J.N., Humler, E., Mével, C., Albarède, F., 2007. Isotopic portrayal of the Earth's upper mantle flow field. Nature 447 (7148), 1069–1074. https://doi.org/10.1038/nature05920.
Meyzen, C.M., Ludden, J.N., Humler, E., Luais, B., Toplis, M.J., Mével, C., Storey, M., 2005. New insights into the origin and distribution of the DUPAL isotope anomaly in the Indian Ocean mantle from MORB of the Southwest Indian Ridge. Geochem. Geophys. Geosyst. 6 (11). https://doi.org/10.1029/2005GC000979.
Michael, P.J., Schilling, J.-G., 1989. Chlorine in mid-ocean ridge magmas: evidence for assimilation of seawater-influenced components. Geochim. Cosmochim. Acta 53 (12), 3131–3143. https://doi.org/10.1016/0016-7037(89)90094-X.
Patriat, P., Segoufin, J., 1988. Reconstruction of the central Indian Ocean. Tectonophysics 155 (1–4), 211–234. https://doi.org/10.1016/0040-1951(88)90267-3.
Plank, T., Langmuir, C.H., 1998. The chemical composition of subducting sediment and its consequences for the crust and mantle. Chem. Geol. 145 (3), 325–394. https://doi.org/10.1016/S0009-2541(97)00150-2.
Rehka, M., Hofmann, A., 1997. Recycled ocean crust and sediment in Indian Ocean MORB. Earth Planet. Sci. Lett. 147 (1–4), 93–106. https://doi.org/10.1016/S0012-821X(97)00009-5.
Reid, I., Jackson, H., 1981. Oceanic spreading rate and crustal thickness. Mar. Geophys. Res. 5 (2), 165–172. https://doi.org/10.1007/BF00163477.
Rudnick, R., Gao, S., Holland, H., Turekian, K., 2003. Composition of the continental crust. In: The Crust, vol. 3, pp. 1–64.
Rudnick, R.L., Fountain, D.M., 1995. Nature and composition of the continental crust: a lower crustal perspective. Rev. Geophys. 33 (3), 267–309. https://doi.org/10.1029/95RG01302.
Simon, N.S., Carlson, R.W., Pearson, D.G., Davies, G.R., 2007. The origin and evolution of the Kaapvaal cratonic lithospheric mantle. J. Petrol. 48 (3), 589–625. https://doi.org/10.1093/petrology/egl074.
Standish, J.J., Sims, K.W., 2010. Young off-axis volcanism along the ultraslow-spreading Southwest Indian Ridge. Nat. Geosci. 3 (4), 286–292. https://doi.org/10.1038/ngeo824.
Storey, M., Mahoney, J.J., Saunders, A.D., 1997. Cretaceous Basalts in Madagascar and the Transition between Plume and Continental Lithosphere Mantle Sources. Geophysical Monograph, vol. 100. American Geophysical Union, pp. 95–122.
Stracke, A., Bizimis, M., Salters, V.J., 2003. Recycling oceanic crust: quantitative constraints. Geochem. Geophys. Geosyst. 4 (3). https://doi.org/10.1029/2001GC000223.
Stracke, A., Hofmann, A.W., Hart, S.R., 2005. FOZO, HIMU, and the rest of the mantle zoo. Geochem. Geophys. Geosyst. 6 (5). https://doi.org/10.1029/2004GC000824.
Sun, S.S., McDonough, W.F., 1989. Chemical and Isotopic Systematics of Oceanic Basalts: Implications for Mantle Composition and Processes. Special Publications, vol. 42(1). Geological Society, London, pp. 313–345.
Tatsumi, Y., 2000. Continental crust formation by crustal delamination in subduction zones and complementary accumulation of the enriched mantle I component in the mantle. Geochem. Geophys. Geosyst. 1 (12). https://doi.org/10.1029/2000GC000094.
Vervoort, J.D., Patchett, P.J., Albarède, F., Blichert-Toft, J., Rudnick, R., Downes, H., 2000. Hf–Nd isotopic evolution of the lower crust. Earth Planet. Sci. Lett. 181 (1–2), 115–129. https://doi.org/10.1016/S0012-821X(00)00170-9.
Vervoort, J.D., Plank, T., Prytulak, J., 2011. The Hf–Nd isotopic composition of marine sediments. Geochim. Cosmochim. Acta 75 (20), 5903–5926. https://doi.org/10.1016/j.gca.2011.07.046.
Willbold, M., Stracke, A., 2010. Formation of enriched mantle components by recycling of upper and lower continental crust. Chem. Geol. 276 (3–4), 188–197. https://doi.org/10.1016/j.chemgeo.2010.06.005.
Woelki, D., Haase, K.M., Schoenhofen, M.V., Beier, C., Regelous, M., Krumm, S.H., Günther, T., 2018. Evidence for melting of subducting carbonate-rich sediments in the western Aegean Arc. Chem. Geol. 483, 463–473. https://doi.org/10.1016/j.chemgeo.2018.03.014.
Zhou, H., Dick, H.J., 2013. Thin crust as evidence for depleted mantle supporting the Marion Rise. Nature 494 (7436), 195–200. https://doi.org/10.1038/nature11842.
Zindler, A., Hart, S., 1986. Chemical geodynamics. Annu. Rev. Earth Planet. Sci. 14 (1), 493–571.